Journal of Power Sources 188 (2009) 213–219

Contents lists available at ScienceDirect

Journal of Power Sources

journal homepage: www.elsevier.com/locate/jpowsour

Comparison of current distributions in proton exchange membrane fuel cells with interdigitated and serpentine flow fields

Guangsheng Zhang[a], Liejin Guo[a], Bin Ma[a], Hongtan Liu[a,b,*]

[a] State Key Laboratory of Multiphase Flow in Power Engineering, Xi'an Jiaotong University, Xi'an, Shaanxi 710049, China
[b] Department of Mechanical and Aerospace Engineering, University of Miami, Coral Gables, FL 33124, USA

ARTICLE INFO

Article history:
Received 22 September 2008
Received in revised form 22 October 2008
Accepted 23 October 2008
Available online 31 October 2008

Keywords:
Proton exchange membrane
Fuel cell
Current distribution
Flow fields

ABSTRACT

Current distributions in a proton exchange membrane fuel cell (PEMFC) with interdigitated and serpentine flow fields under various operating conditions are measured and compared. The measurement results show that current distributions in PEMFC with interdigitated flow fields are more uniform than those observed in PEMFC with serpentine flow fields at low reactant gas flow rates. Current distributions in PEMFC with interdigitated flow fields are rather uniform under any operating conditions, even with very low gas flow rates, dry gas feeding or over-humidification of reactant gases. Measurement results also show that current distributions for both interdigitated and serpentine flow fields are significantly affected by reactant gas humidification, but their characteristics are different under various humidification conditions, and the results show that interdigitated flow fields have stronger water removal capability than serpentine flow fields. The optimum reactant gas humidification temperature for interdigitated flow fields is higher than that for serpentine flow fields. The performance for interdigitated flow fields is better with over-humidification of reactant gases but it is lower when air is dry or insufficiently humidified than that for serpentine flow fields.

1. Introduction

As non-uniform current distribution in proton exchange membrane fuel cell (PEMFC) can result in poor reactant and catalyst utilization, reduced energy efficiency and possible corrosion processes in the cell [1], measurement of current distribution can provide valuable information for optimization of operation and design of PEMFC. Therefore, great efforts have been made to measure current distributions in PEMFCs and various methods have been developed to measure current distributions in the past decade since the pioneering work by Cleghorn et al. [1] and Stumper et al. [2].

Segmenting flow field/current collector, mostly in the anode side, is the most popular approach to measuring the current distribution in PEMFCs. This approach was first demonstrated by Cleghorn et al. [1], who fabricated a segmented anode flow field using printed circuit board (PCB) technology in the late 1990s. Anode gas diffusion layer (GDL) and catalyst layer (CL) were also segmented in their work to avoid lateral currents. Because segmenting membrane electrode assembly (MEA) is complicated and may influence the true fuel cell operation characteristics, segmented MEA was rarely used in later researches [3–31]. The calculation by Noponen et al. [4] showed that the distortion of current distribution resulting from non-segmenting of GDL is tolerable.

With a method similar to that of Cleghorn et al. [1], Brett et al. [3] measured the current distribution along the length of a single flow channel in a PEMFC with higher spatial and time resolution, and they observed the time delay of local currents after inlet reactant gas changes due to the mass transport of gas through GDL. Noponen et al. [4–6] embedded gold-plated stainless steel ribs into an insulating plastic slab to create a segmented flow field and studied current distributions under various operating conditions in free-breathing PEMFCs. Noponen et al. [7] also used the techniques of segmenting flow field/current collector to measure current distributions in a PEMFC with net flow geometry.

Segmenting flow field approach was also adopted by Mench et al. [8–10] and Yang et al. [11] in their research, and particularly, they managed to measure the species distribution and current distribution simultaneously [10,11]. Hakenjos et al. [12–14] not only

* Corresponding author at: Department of Mechanical and Aerospace Engineering, University of Miami, Coral Gables, FL 33124, USA. Tel.: +1 305 284 2019; fax: +1 305 284 2580.
E-mail addresses: hongtanliu@mail.xjtu.edu.cn, hliu@miami.edu (H. Liu).

0378-7753/$ – see front matter © 2009 Published by Elsevier B.V.
doi:10.1016/j.jpowsour.2008.10.074

measured the current distribution, but also measured the temperature distribution on the MEA surface with infrared thermography [12–14] and localized impedance spectra [13,14]. Natarajan and Van Nguyen [15–17], Araki et al. [18,19] as well as Eckl et al. [20] used segmented approach in their research for current distribution measurement, and more importantly, they used numerical simulation to compare with or assist interpretation of the experimental results [17–20]. Ghosh et al. [21,22] developed a semi-segmented current collector method which has an advantage of measuring current distributions in a single cell as well as in a stack at any desired position.

Based on magnetic effects of current, Hall sensors were used to refine the segmenting flow field approach. The application of Hall sensors was first demonstrated by Wieser et al. [23], who used an array of Hall sensors inside the segmented flow field to measure current distributions. Hall sensors were later put outside of PEMFC to facilitate current measurement and enhance accuracy by following researchers [24–28]. Bender et al. [24] used Hall sensors to refine the segmented flow field approach by Cleghorn et al. [1], which eliminated the necessity of using two electronic loads and made the system able to measure the different local currents simultaneously. Similar methods were developed by Yoon et al. [25], Geiger et al. [26,27] and Strickland et al. [28].

Sun et al. [29,30] and Zhang et al. [31] developed a current distribution measurement gasket method, which is essentially segmenting approach, and this method has a particular advantage of no need to modify any component of the experimental fuel cell.

Subcell configuration is another popular approach where electrically isolated subcells that can be controlled independently are placed at various locations in the MEA. It was first developed by Stumper et al. [2], who also demonstrated the other two methods: the partial MEA method with low spatial resolution and the current mapping technique with a passive resistor network. The subcell approach was then modified and employed by Rajalakshmi et al. [32], Wu et al. [33] and Liu et al. [34], with more sophisticated cell designs to study current distributions in PEMFCs.

There are also some other approaches to measuring current distributions in PEMFCs with special features. Hauer et al. [35] developed a magnetotomography-based method, which is non-invasive and has virtually no feedback effect on the test object and the current distribution to be measured. Freunberger et al. [36,37] measured the potential distribution at the interface between GDL and CL and realized sub-millimeter resolution of current distribution measurement. Wang and Liu [38] developed a novel yet simple approach to directly measure the current densities under the channel and the shoulder separately. Their measurement results [35–38] presented detailed information of current distribution under the ribs and channels. The experimental data in Ref. [36] was used by Li et al. [39] to validate their model. Wilkinson et al. [40] managed to determine current distribution indirectly by measuring temperature distributions based on the correlation of local temperature with local current density.

The current distribution measurement methods mentioned above have been demonstrated in PEMFCs with serpentine or parallel flow fields and numerous interesting results have been obtained [1,2,4,9,13,23,30,35,36,38,40]. Compared with serpentine or parallel flow fields, interdigitated flow fields can provide better water management and reactant transport under some operating conditions [41,42] and were expected to lead to more uniform current distributions. But no experimental results on the current distributions in PEMFC with interdigitated flow fields have been found in the literature. Thus, the objective of this work is to investigate the characteristics of current distributions in PEMFCs with interdigitated flow fields. To better understand the characteristics, comparisons with serpentine flow fields are also to be made. To ensure proper comparisons, both interdigitated and serpentine flow field plats (FFPs) were designed and manufactured in this study. The two patterns of FFPs have the same geometric parameters and all the experimental conditions were kept the same. Then the current distributions in PEMFC with both interdigitated and serpentine flow fields were measured and compared.

Table 1
Geometric parameters of the experimental fuel cell.

Channel length (mm)	40
Channel width (mm)	1
Main channel width (interdigitated) (mm)	2
Channel depth (mm)	1
Shoulder width (mm)	1
Number of channels	20
Number of shoulders	19
MEA active area (cm^2)	16
Membrane thickness (mm)	0.05
CL thickness (mm)	0.01
GDL thickness (mm)	0.28

2. Experimental

2.1. Experimental fuel cell assembly

The two pairs of graphite FFPs with two different flow fields were manufactured and used with the same single fuel cell hardware in Ref. [29]. For each flow pattern, the flow field in the cathode is identical to that in the anode and parallel flow (co-flow) is used. Geometric parameters of the two patterns of flow fields are the same to ensure appropriate comparison of current distributions. Channel widths, channel depths and shoulder widths are all 1 mm. There are 20 channels and 19 shoulders in every FFP, and the active area of the MEA is 4 cm × 4 cm. Details of the geometric parameters of the FFPs are shown in Table 1.

All the MEAs used in this study were the same, consisting of Nafion® 112 as the proton exchange membrane sandwiched between catalyst-loaded Toray® carbon paper (TGP-H-090) GDLs with porosity of 78% [43]. The catalyst loading was 0.4 mg Pt cm^{-2} on both anode and cathode. Geometric parameters of the MEAs are also shown in Table 1.

2.2. Current distribution measurement method

The current distribution measurement gasket technique developed by Sun et al. [29] was used to measure and compare the current distributions in PEMFCs with interdigitated and serpentine flow fields. Fig. 1 shows schematically the PEMFC current distribution measurement system. Details of how the technique works can be found in Ref. [29]. Considering that hydrogen in anode transfers and reacts much faster than oxygen in the air in cathode, in this study the current distribution measurement gasket was placed in the anode side to minimize the effects of the gasket on cell performance. The gasket was inserted between the anode GDL and the anode FFP. Fig. 2 is a photograph of current distribution measurement gasket on the interdigitated FFP.

2.3. Treatment of experimental data

There are 19 shoulders in the FFP, and correspondingly, 19 local currents of the PEMFC were measured. The shoulders and corresponding local currents were numbered from 1 to 19 in the direction from gas inlet to gas outlet (from top to bottom in Fig. 2). Similar

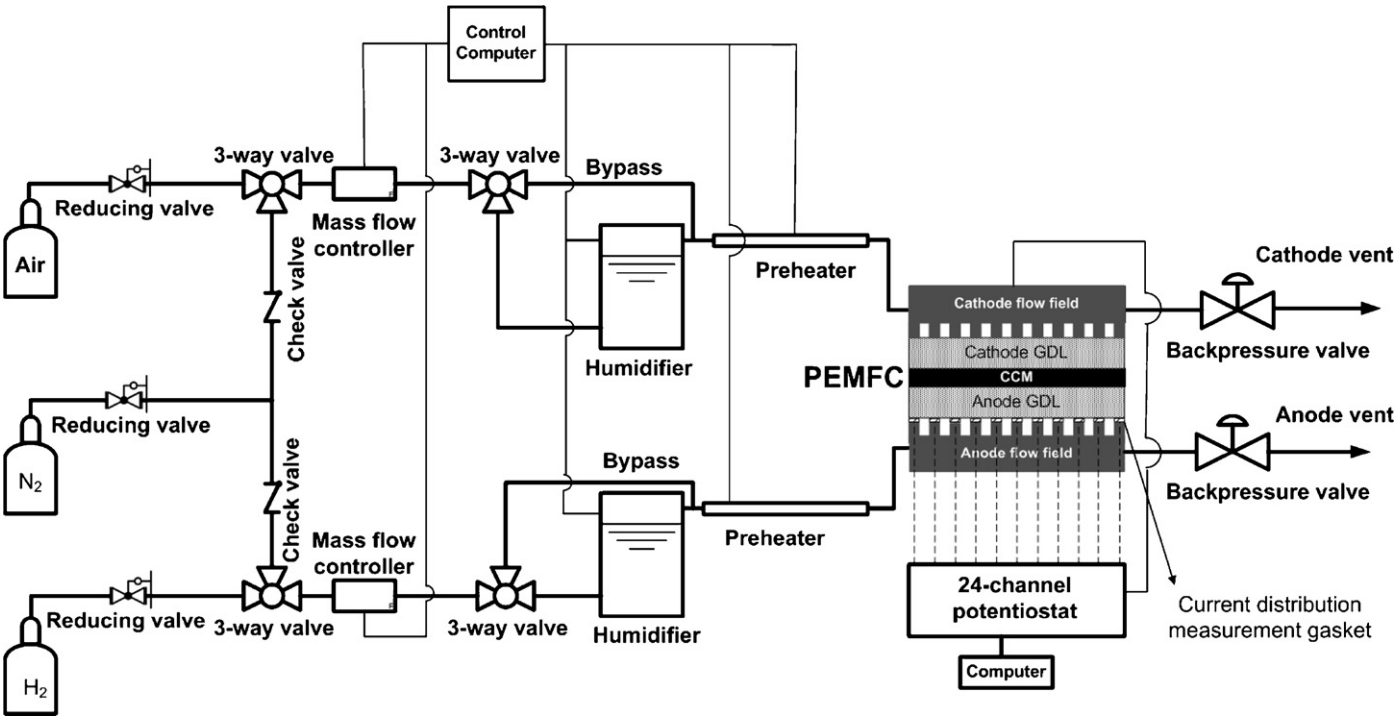

Fig. 1. Schematic diagram of the PEMFC current distribution measurement system.

to what was done by Sun et al. [29], local currents from shoulders number 1 and number 19 were not used in the presented results because they cover larger active areas than the rest. Every other shoulder collects current from one shoulder and two half-channels, which represent an active area of 0.8 cm^2. Therefore, the local current density can be calculated from measured local current divided by the area of 0.8 cm^2.

Similar to experimental results in some previous work [1,3,9,32,34], the original current distribution curves are not very smooth, as is shown in Fig. 3. To focus on the trends of current distribution, the local "noise" of the original experimental data was eliminated by averaging each point with its two neighboring points.

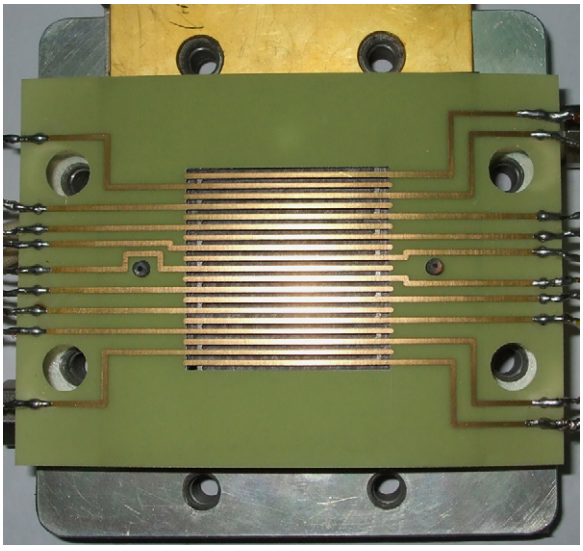

Fig. 2. Photograph of the current distribution measurement gasket set on the anode interdigitated FFP.

Fig. 3 shows sample experimental results before and after the data treatment.

3. Results and discussion

Operating conditions, including reactant gas flow rates, fuel cell temperature, reactant gas humidification, etc., have significant effects on current distributions in PEMFCs, as were demonstrated in previous work [9,29,30]. Therefore, the current distributions in PEMFCs with interdigitated and serpentine flow fields under various operating conditions were investigated. Basic operating parameters were set to be the same for all the experiments. Air flow rate is 1200 sccm, which is equivalent to 4.5 A cm^{-2}. Hydrogen flow rate is 200 sccm, which is equivalent to 1.8 A cm^{-2}. Cell operating temperature, air humidification and hydrogen humidification temperatures are all 333 K. Backpressure is kept at 1 atm for all the experiments.

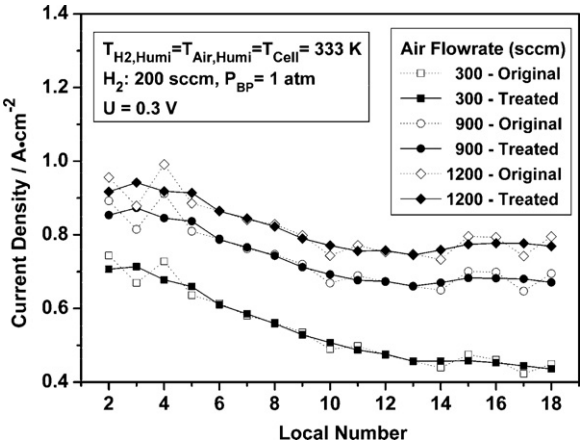

Fig. 3. A sample of experimental data treatment.

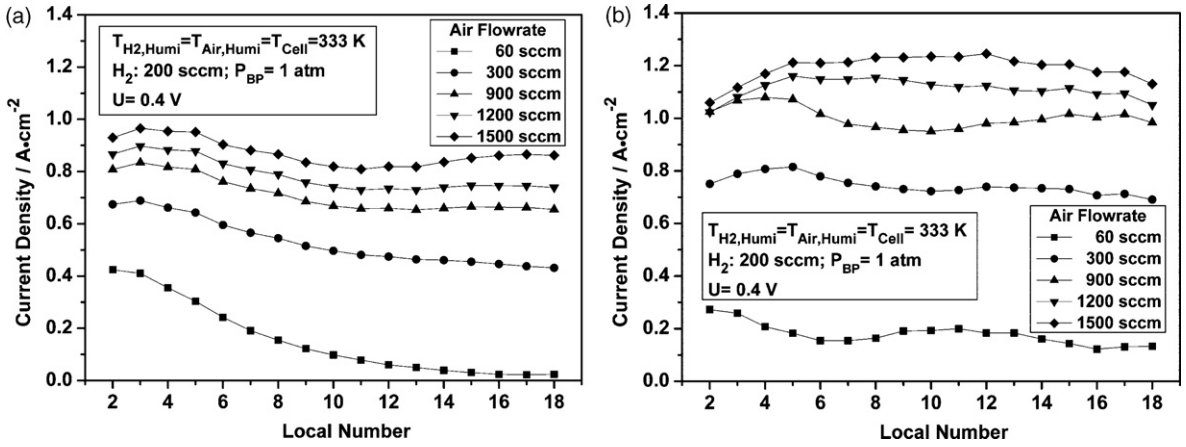

Fig. 4. (a) Current distributions in the PEMFC with serpentine flow fields at different air flow rates and (b) current distributions in the PEMFC with interdigitated flow fields at different air flow rates.

3.1. Current distributions at various air flow rates

Current distributions in PEMFCs with serpentine and interdigitated flow fields at various air flow rates are shown in Fig. 4a and b, respectively. It can be seen that local current densities keep increasing as air flow rate increases from 60 to 1500 sccm for both serpentine and interdigitated flow fields, which is mainly due to higher oxygen concentration with increased air flow rate. From comparison of Fig. 4a and b, it is easy to find that current distributions are more uniform in PEMFC with interdigitated flow fields at low air flow rates. As is shown in Fig. 4a, for serpentine flow fields, local current densities generally decrease from the inlet to outlet due to decreased oxygen concentration. When the air flow rate was as low as 60 sccm, the local current densities near the outlet were almost zero. However, it can be seen from Fig. 4b that for interdigitated flow fields, at low air flow rate of 60 sccm, the current distribution is still rather uniform.

3.2. Current distributions at various hydrogen flow rates

Fig. 5a and b show current distributions at various hydrogen flow rates. It can be seen that the local current densities increase with increasing hydrogen flow rate for both serpentine and interdigitated flow fields. Comparing Fig. 5a with b, it is obvious that current distributions of the two patterns of flow fields are very different. For serpentine flow fields, as is shown in Fig. 5a, local current densities near the inlet change little as the hydrogen flow rate increases from 60 to 300 sccm, which is due to high diffusivity and quick reaction kinetics of hydrogen. And when hydrogen is insufficient at flow rate of 60 sccm, the current distribution curve drops sharply near the outlet where hydrogen is being depleted. For interdigitated flow fields, however, according to Fig. 5b, local current densities near the inlet increase considerably as the hydrogen flow rate increases and local current densities near the outlet are not lower than those near the inlet for all hydrogen flow rates including the very low flow rate at 60 sccm. These results show that interdigitated flow fields have more uniform current distributions.

The results shown in Figs. 4 and 5 demonstrate clearly that the current distributions in PEMFC with interdigitated flow fields are much more uniform than that with serpentine flow fields, particularly at low reactant gas flow rates. This can be attributed to more uniform reactant gas distributions in interdigitated flow fields. In a serpentine flow field, the reactant flows from inlet to outlet and each area along the channel is hydraulically connected in series. Thus the reactant concentration and local current density usually decreases along the channel. In an interdigitated flow field, since the pressure drop across each land area is much higher than those along feeder channels or collector channels, all the channels are essentially hydraulically connected in parallel. There is hardly any up-stream or down-stream effect and all the channels have similar current density due to their similar

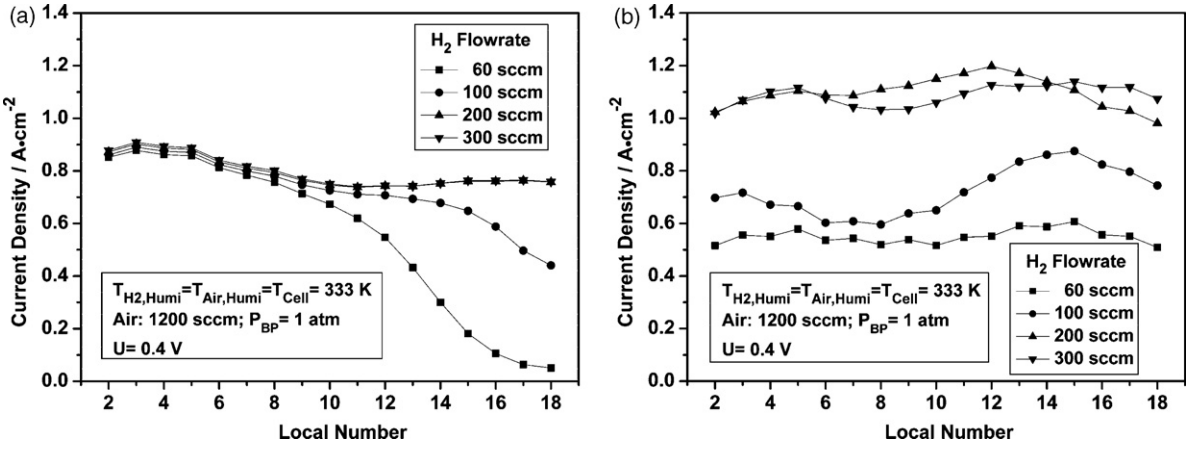

Fig. 5. (a) Current distributions in the PEMFC with serpentine flow fields at different hydrogen flow rates and (b) current distributions in the PEMFC with interdigitated flow fields at different hydrogen flow rates.

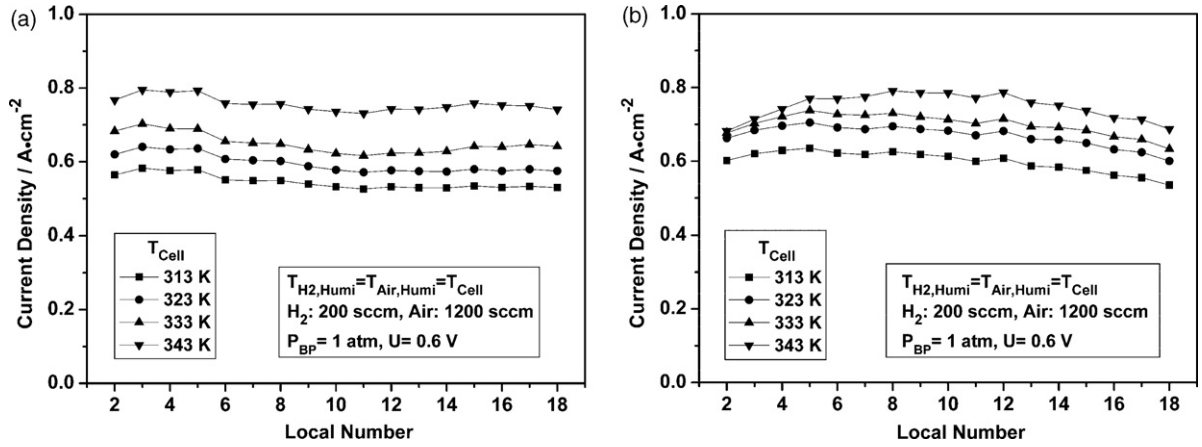

Fig. 6. (a) Current distributions in the PEMFC with serpentine flow fields at different cell operating temperatures and (b) current distributions in the PEMFC with interdigitated flow fields at different cell operating temperatures.

reactant flows and concentrations. Obviously, the higher pressure drop occurred in an interdigitated flow field make it not suitable for every application despite its advantage of uniform current distributions.

3.3. Current distributions at various cell operating temperatures

Current distributions in the experimental fuel cells operated at different temperatures were also measured and the results are shown in Fig. 6a and b [31], where both hydrogen and air humidification temperatures are equal to the cell operating temperature. It can be seen, as expected, that the local current densities increase with increasing cell operating temperature for both serpentine and interdigitated flow fields.

3.4. Current distributions at various air humidification temperatures

Water plays an important role in both overall and local performance of PEMFC, and reactant gases are usually humidified to ensure proper hydration of the membranes. Fig. 7a and b [31] shows the current distributions at different air humidification temperatures for serpentine and interdigitated flow fields, respectively. It can be easily seen that air humidification has significant effects on current distributions in PEMFC with both serpentine and interdigitated flow fields. All the local performances are very poor when air is dry or not sufficiently humidified, while all the local performances reach optimum when air is fully humidified.

It is also easy to notice that the current distribution characteristics of PEMFC with interdigitated flow fields are different from that with serpentine flow fields. First, as shown in Fig. 7a, local performances of PEMFC with serpentine flow fields reach optimum when air humidification temperature is 323 K, 10 K lower than cell operating temperature. Further increase in air humidification temperature (333, 343 and 353 K) leads to lower overall and local performance, which could be attributed to water flooding. While for PEMFC with interdigitated flow fields, as shown in Fig. 7b, local performances reach optimum when air humidification temperature is 333 K, equal to the cell temperature. Further increase in air humidification temperature has no apparent effect on both the overall and local performances and current distributions for over-humidification cases are almost the same as the optimum performance when air is humidified at 333 K. These results can be attributed to the stronger water removal capability of interdigitated flow fields.

Second, it is easy to find that when air is fully humidified or over humidified, the local current densities with interdigitated flow fields are no lower than those with serpentine flow fields, whereas when air is not humidified or insufficiently humidified, the local current densities with interdigitated flow fields are much lower than those with serpentine flow fields. For example, in the case of no-humidification, even the highest local current density with

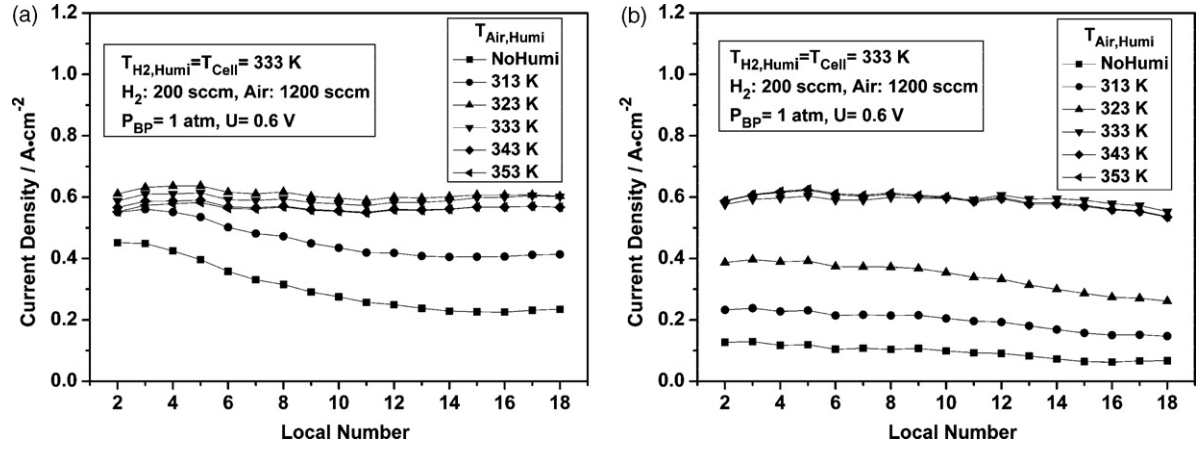

Fig. 7. (a) Current distributions in the PEMFC with serpentine flow fields at different air humidification temperatures and (b) current distributions in the PEMFC with interdigitated flow fields at different air humidification temperatures.

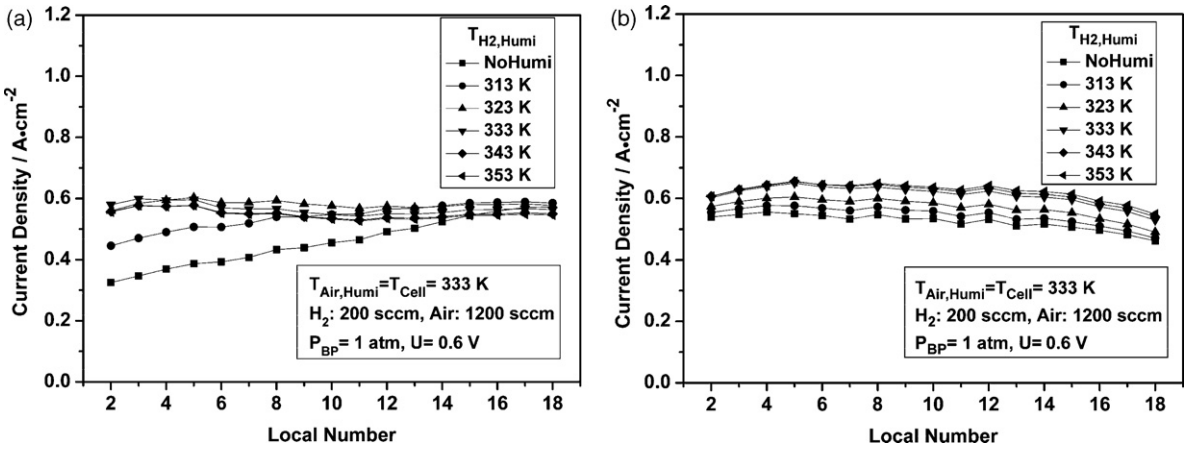

Fig. 8. (a) Current distributions in the PEMFC with serpentine flow fields at different hydrogen humidification temperatures and (b) current distributions in the PEMFC with interdigitated flow fields at different hydrogen humidification temperatures.

interdigitated flow fields (local number 2 shown in Fig. 7b) is much lower than the lowest local current density with serpentine flow fields (local number 16, near the outlet, shown in Fig. 7a). This phenomenon is again due to the stronger water removal capability of interdigitated flow fields, except that under such conditions, this stronger capability becomes detrimental rather than beneficial. When air is not sufficiently humidified or not humidified at all, the membrane is easily to be dried. Stronger water removal capability of interdigitated flow fields due to convection accelerate the drying of the membrane, leading to worse performance.

Finally, it is interesting to note that current distribution curves in Fig. 7a (serpentine flow fields) decrease from the inlet to outlet when air is not humidified or insufficiently humidified at 313 K. This could be caused by the net water transport from anode to cathode. Since air in the cathode is far from saturated and has a large flow rate, the net water transfer from the anode to the cathode is higher, leading to worse dehydration of the membrane near the anode side. This problem becomes more serious along the flow direction, and therefore results in decreasing local current densities.

3.5. Current distributions at various hydrogen humidification temperatures

Fig. 8a and b [31] shows the effects of hydrogen humidification on current distributions in PEMFC with serpentine and interdigitated flow fields, respectively. It can be seen that the effects of hydrogen humidification are similar to those of air humidification for both serpentine and interdigitated flow fields.

First, for serpentine flow fields, local performances improve with increasing hydrogen humidification from no humidification to humidification temperature at 323 K, but further increase of hydrogen humidification leads to lower performance. For interdigitated flow fields, local performances reach optimum when hydrogen humidification temperature is increased to 333 K and then keep almost unchanged with over-humidification. Which is again due to the fact that increased humidification mitigates the drying of the membrane when humidification is insufficient and that stronger water removal capability of interdigitated flow fields eliminates the flooding problem caused by over-humidification.

Second, it can be found that the current distribution curves in Fig. 8a and b are closer together than those in Fig. 7a and b, respectively, indicating that the effects of hydrogen humidification on current distribution are not as significant as those of air humidification for both serpentine and interdigitated flow fields. This is due to the fact that the membrane is so thin that water can easily diffuse from the cathode back to the anode to mitigate the drying of the membrane, and that hydrogen flow rates are much lower than air flow rates in these experiments and have much weaker water removal ability.

Finally, it is worthwhile to note that when hydrogen is not humidified or insufficiently humidified, as is shown in Fig. 8a, local current densities start low from the inlet and increase along the flow direction. This could be attributed to the fact that back diffusion of water from the cathode to the anode increases along the flow direction as more water is produced along the flow direction, which improves the hydration of the membrane. In comparison, current distributions in PEMFC with interdigitated flow fields, as can be seen from Fig. 8b, are rather uniform when hydrogen is not humidified or insufficiently humidified, which can be attributed to the more uniform distribution of reactant gas and water.

4. Conclusions

Current distributions in a PEMFC with both interdigitated and serpentine flow fields were measured and the results at various reactant gas flow rates, cell operating temperatures and reactant gas humidification temperatures were compared. The following conclusions can be drawn from this study.

Current distributions in PEMFC with interdigitated flow fields are more uniform than those with serpentine flow fields at low reactant gas flow rates. Current distributions in PEMFC with interdigitated flow fields are rather uniform under any operating conditions, even with very low gas flow rates, dry gas feeding, or over-humidification of reactant gases. Uniform current distributions with interdigitated flow fields can be attributed to the uniform distribution of reactant gas and water.

Similar to PEMFC with serpentine flow fields, current distributions in PEMFC with interdigitated flow fields are also significantly affected by reactant gas humidification. But the effects for interdigitated flow fields are different from those for serpentine flow fields due to their stronger water removal capability, which plays a complicated role. On the one hand, the stronger water removal capability leads to higher optimum reactant gas humidification temperature and ensures that the current distributions with over-humidification of reactant gases are just as good as the optimal humidification. On the other hand, the stronger water removal capability results in very poor performance when air is dry or insufficiently humidified.

Acknowledgments

Financial supports from Chang Jiang Scholars Program of the Ministry of Education of China, NSFC Fund for Creative Research Groups (Grant No. 50521604) and NSFC Key Project (Grant No. 50536020) are gratefully appreciated. The authors thank Mr. Lizhong Ma for assistance in experiment and Dr. Hong Sun for useful discussions.

References

[1] S.J.C. Cleghorn, C.R. Derouin, M.S. Wilson, S. Gottesfeld, J. Appl. Electrochem. 28 (1998) 663–672.
[2] J. Stumper, S.A. Campbell, D.P. Wilkinson, M.C. Johnson, M. Davis, Electrochim. Acta 43 (1998) 3773–3783.
[3] D.J.L. Brett, S. Atkins, N.P. Brandon, V. Vesovic, N. Vasileiadis, A.R. Kucernak, Electrochem. Commun. 3 (2001) 628–632.
[4] M. Noponen, T. Mennola, M. Mikkola, T. Hottinen, P. Lund, J. Power Sources 106 (2002) 304–312.
[5] M. Noponen, T. Hottinen, T. Mennola, M. Mikkola, P. Lund, J. Appl. Electrochem. 32 (2002) 1081–1089.
[6] T. Hottinen, M. Noponen, T. Mennola, O. Himanen, M. Mikkola, P. Lund, J. Appl. Electrochem. 33 (2003) 265–271.
[7] M. Noponen, J. Ihonen, A. Lundblad, G. Lindbergh, J. Appl. Electrochem. 34 (2004) 255–262.
[8] M.M. Mench, C.Y. Wang, J. Electrochem. Soc. 150 (2003) A79–A85.
[9] M.M. Mench, C.Y. Wang, M. Ishikawa, J. Electrochem. Soc. 150 (2003) A1052–A1059.
[10] Q. Dong, M.M. Mench, S. Cleghorn, U. Beuscher, J. Electrochem. Soc. 152 (2005) A2114–A2122.
[11] X.G. Yang, N. Burke, C.Y. Wang, K. Tajiri, K. Shinohara, J. Electrochem. Soc. 152 (2005) A759–A766.
[12] A. Hakenjos, H. Muenter, U. Wittstadt, C. Hebling, J. Power Sources 131 (2004) 213–216.
[13] A. Hakenjos, C. Hebling, J. Power Sources 145 (2005) 307–311.
[14] W.H.J. Hogarth, J. Steiner, J.B. Benziger, A. Hakenjos, J. Power Sources 164 (2007) 464–471.
[15] D. Natarajan, T. Van Nguyen, AIChE J. 51 (2005) 2587–2598.
[16] D. Natarajan, T. Van Nguyen, AIChE J. 51 (2005) 2599–2608.
[17] D. Natarajan, T. Van Nguyen, J. Power Sources 135 (2004) 95–109.
[18] T. Araki, H. Koori, T. Taniuchi, K. Onda, J. Power Sources 152 (2005) 60–66.
[19] K. Onda, T. Araki, T. Taniuchi, D. Sunakawa, K. Wakahara, M. Nagahama, J. Electrochem. Soc. 154 (2007) B247–B257.
[20] R. Eckl, R. Grinzinger, W. Lehnert, J. Power Sources 154 (2006) 171–179.
[21] P.C. Ghosh, T. Wuster, H. Dohle, N. Kimiaie, J. Mergel, D. Stolten, J. Power Sources 154 (2006) 184–191.
[22] P.C. Ghosh, T. Wuster, H. Dohle, N. Kimiaie, J. Mergel, D. Stolten, J. Fuel Cell Sci. Technol. 3 (2006) 351–357.
[23] C. Wieser, A. Helmbold, E. Gulzow, J. Appl. Electrochem. 30 (2000) 803–807.
[24] G. Bender, M.S. Wilson, T.A. Zawodzinski, J. Power Sources 123 (2003) 163–171.
[25] Y.G. Yoon, W.Y. Lee, T.H. Yang, G.G. Park, C.S. Kim, J. Power Sources 118 (2003) 193–199.
[26] A.B. Geiger, R. Eckl, A. Wokaun, G.G. Scherera, J. Electrochem. Soc. 151 (2004) A394–A398.
[27] F.N. Buchi, A.B. Geiger, R.P. Neto, J. Power Sources 145 (2005) 62–67.
[28] D.G. Strickland, S. Litster, J.G. Santiago, J. Power Sources 174 (2007) 272–281.
[29] H. Sun, G. Zhang, L. Guo, H. Liu, J. Power Sources 158 (2006) 326–332.
[30] H. Sun, G. Zhang, L. Guo, D. Shang, H. Liu, J. Power Sources 168 (2007) 400–407.
[31] G. Zhang, B. Ma, D. Shang, L. Guo, H. Sun, H. Liu, ECS Trans. 11 (2007) 1545–1552.
[32] N. Rajalakshmi, M. Raja, K.S. Dhathathreyan, J. Power Sources 112 (2002) 331–336.
[33] J.F. Wu, B.L. Yi, M. Hou, Z.J. Hou, H.M. Zhang, Electrochem. Solid State Lett. 7 (2004) A151–A154.
[34] Z.X. Liu, Z.Q. Mao, B. Wu, L.S. Wang, V.M. Schmidt, J. Power Sources 141 (2005) 205–210.
[35] K.-H. Hauer, R. Potthast, T. Wuster, D. Stolten, J. Power Sources 143 (2005) 67–74.
[36] S.A. Freunberger, M. Reum, J. Evertz, A. Wokaun, F.N. Buchi, J. Electrochem. Soc. 153 (2006) A2158–A2165.
[37] S.A. Freunberger, M. Reum, A. Wokaun, F.N. Buchi, Electrochem. Commun. 8 (2006) 1435–1438.
[38] L. Wang, H.T. Liu, J. Power Sources 180 (2008) 365–372.
[39] J. Li, C.Y. Wang, A. Su, J. Electrochem. Soc. 155 (2008) B64–B69.
[40] M. Wilkinson, M. Blanco, E. Gu, J.J. Martin, D.P. Wilkinson, J.J. Zhang, H. Wang, Electrochem. Solid State Lett. 9 (2006) A507–A511.
[41] D.L. Wood, Y.S. Yi, T.V. Nguyen, Electrochim. Acta 43 (1998) 3795–3809.
[42] J.S. Yi, T.V. Nguyen, J. Electrochem. Soc. 146 (1999) 38–45.
[43] Toray carbon paper product information, URL: http://www.torayca.com/index2.html.